Impact of Bio-alcohol Fuels Combustion on Particulate Matter (PM) Morphology from Efficient Gasoline Direct Injection Engines

Hergueta Santos-Olmo, Cruz; Tsolakis, Athanasios; Herreros, Jose; Bogarra Macias, Maria; Price, Emily; Simmance, K; York, Andrew; Thompsett, D

DOI:
doi.org/10.1016/j.apenergy.2018.08.076

Document Version
Peer reviewed version

Citation for published version (Harvard):
Hergueta Santos-Olmo, C, Tsolakis, A, Herreros, J, Bogarra Macias, M, Price, E, Simmance, K, York, A & Thompsett, D 2018, 'Impact of Bio-alcohol Fuels Combustion on Particulate Matter (PM) Morphology from Efficient Gasoline Direct Injection Engines', *Applied Energy*, vol. 230, pp. 794-802. https://doi.org/doi.org/10.1016/j.apenergy.2018.08.076

Impact of Bio-alcohol Fuels Combustion on Particulate Matter Morphology from Efficient Gasoline Direct Injection Engines

Hergueta C. [1], Tsolakis A. [1]*, Herreros J.M.[1], Bogarra M. [1], Price E. [2], Simmance K. [2], York A.P.E. [2] and Thompsett D. [2]

[1]*Mechanical Engineering, University of Birmingham, B15 2TT, Birmingham, UK;*

[2] *Johnson Matthey Technology Centre, Blount's Court, Sonning Common, Reading, RG4 9NH, UK*

Email: a.tsolakis@bham.ac.uk

Abstract

The requirements for controlling particulate emissions in gasoline direct injection (GDI) engines, particularly in hybrid vehicles (where frequent cold-start event impact on both, particles characteristics and catalytic aftertreament efficiency), nesesitates the need for understanding their formation mechanism and their morphological characteristics. The findings described in this investigation have significance in the design of efficient Gasoline Particulate Filters (GPFs) and the development of computational models that predict particle filtration and oxidation processes.

Morphological analysis of the particulate emissions from the combustion of commercial gasoline and two bio-alcohol blends: of 25% v/v ethanol in gasoline and 33% v/v butanol and 67% v/v gasoline, in a modern GDI engine has been carried out using a transmission electron microscopy. The primary particle size distribution from the combustion of butanol-gasoline blend was slightly smaller compared to gasoline, while the mean primary particle diameter was 3 nm smaller from the combustion of ethanol-gasoline fuel. This decrease in primary particle size for ethanol-gasoline blend was also reflected in a reduction of the mean radius of gyration and mean number of primary particles per agglomerate.

The combustion of butanol-gasoline blend induced improved particle oxidation rates during the combustion process and post-oxidation stage, and led in 80% and 60% reduction in particle concentration in the engine exhaust when compared to the combustion of gasoline and ethanol-gasoline blend, respectively. Additionally, the estimation of the particle fractal dimension through the use of fractal equation, minimum bonding rectangle method and root form factor showed comparable results for butanol-gasoline and gasoline, with the particle agglomerates being more compact than the ethanol-gasoline fuel, where more chain like particles are seen. Therefore, particles emitted from the combustion of ethanol-gasoline fuel are easier to be trapped (lower fractal dimension) and present a higher reactivity (high surface/volume ratio) compared to particles emitted from gasoline combustion.

Keywords: Morphology, TEM, Bio-Alcohol, GDI, Particle, Combustion

Introduction

Gasoline Direct Injection (GDI) engine technology enables a reduction in both vehicle fuel consumption and CO_2 emissions [1]. On the other hand, there is an increased production of particulate matter (PM) emissions, particularly during engine cold start and vehicle acceleration [2]. Under such conditions the fuel direct injection process is reported to lead to inhomogeneity of the air-fuel mixture and consequently incomplete fuel combustion, resulting in increased formation of soot [3]. Earlier studies have concluded that particulates in GDI engines are formed due to i) the locally fuel rich regions during the combustion process even in homogeneous mixtures at the macro scale [4], ii) piston wetting that leads to wall fuel-film formation as a consequence of the fuel injection process [5] and, iii) the carbonisation of non-combusted fuel droplets [6, 7]. Factors affecting soot formation are highly related to the chemical structure and thermo-physical properties of the fuel used in combustion process, in addition to local equivalence ratio and in-cylinder temperature.

The Euro 6c regulation restricts the emissions of the particulate number in gasoline engines to $6x10^{11}$ #/km and therefore, several techniques and strategies have been investigated to reduce the level of particulates in GDI vehicles. For instance, the use of exhaust gas recirculation (EGR) in GDI engine has shown reductions of about 20% [8] in overall particulate concentration as a result of the improved fuel economy (i.e. less fuel injected) due to the reduced pumping losses. Gasoline particulate filters (GPFs) can also control particulate emissions, with reported filtration efficiencies of 96-97% for particles below 10 nm [9] and up to 84% of filtration efficiency during the new European driving cycle (NEDC) [10]. Another alternative to reduce particle emission is the use of alternatives fuels. Bogarra et al. [11] and Fennell et al. [12] studied the effect of hydrogen produced in exhaust gas fuel reforming on particles formation in GDI engines. Both the replacement of liquid fuel and the combustion improvements by the addition of hydrogen inhibited particulate formation rates across a wide size range.

The inclusion of oxygenated bio-alcohol fuels in gasoline fuel can reduce PM emissions formation and enhance oxidation during the combustion process. Ethanol and butanol have been proposed as the next generation low-carbon fuels for transportation [13, 14]. The chemical properties of bio-alcohols have been found to be beneficial for reducing PM emissions due to the absence of aromatics, which are potential source of PAHs (polycyclic aromatic hydrocarbons) and soot precursors [15]. In addition, the oxygen content in their molecules promotes particle oxidation and inhibits particle formation rates [16, 17]. However, the literature suggests that the trend of PM emissions formation from the combustion of ethanol-gasoline blends is dependent on the percentage of the ethanol used in the fuel blend and the engine operating (speed/load) conditions. For instance, the higher heat of vaporisation and the low vapour pressure of ethanol can lead to a poorer evaporation compared to gasoline, and therefore, lower quality of air/fuel mixture [18]. The effect of E10 and E20 combustion on the particle size distribution of a wall-guided GDI engine was analysed by Luo et al. [19]. At low

engine load conditions, the combustion of the ethanol/gasoline blends increased both the particle number (PN) and the mean diameter by around 20%. Subsequent increase of the engine load led to 20% reduction in PN and a significant decrease of 20 nm in particle size compared to gasoline. At high engine load conditions, the combination of fuel born oxygen and improved spray pattern of bio-alcohol fuel blends as consequence of the higher fuel injection pressure improved the air/fuel mixture and particulate emissions. Under these conditions the bio-alcohol fuel blend's chemical properties (i.e. oxygen content or low aromatic concentration) predominate over the fuel's physical properties (i.e. higher viscosity). Similar results are reported by He et al. [20] where the combustion of E20 at high engine load of 9 bar IMEP, reduced PN concentration by 20% compared to commercial gasoline. In contrast to the impact of ethanol/gasoline fuel blends on engine out PM emissions, butanol/gasoline blends have shown more consistent trends. Butanol/gasoline blends (B20) have been reported to reduce the concentration of large particles (40-60 nm), but results in the increased concentration of smaller particles 30 nm, with a reduction in the overall total number of particles by 40% [21]. Lattimore et al. [22] also found a significant reduction on particles larger than 50 nm using B20 fuel blend, while a reductions in PN of up to 80% was reported by Hergueta et al. [8] using a B33 fuel blend. The authors attributed this result to the fuel's lower aromatic concentration and higher oxygen content.

In addition to particle size distribution (PSD), transmission electron microscope (TEM) techniques have been used for morphological characterisation. Particle morphology can influence the filtration and regeneration processes of the GPF with an impact on the exhaust backpressure and engine fuel efficiency. Additionally, the porosity and permeability of PM are related to the primary particle diameter and the number of primary particles per agglomerate [23], which directly affect their oxidation reactivity. Primary particle diameters can also provide understanding of the soot oxidation rate as it is dependent on the aggregate surface area to volume ratio. It has been estimated that the aggregate surface area to volume ratio is inversely proportional to primary particle diameter [24]. Physico-chemical properties of biofuels (i.e. ethanol, butanol) are different with respect to gasoline and may modify the PM morphology and alter the soot accumulation and oxidation processes in the GPF. There is a limited number of work to report PM morphology in GDI engines. Recently, M. Bogarra [4] studied PM morphology using baseline gasoline, EGR and hydrogen at engine control unit (ECU) settings and when the fuel injection timing was advanced. Higher PM variability in primary particle diameters at ECU engine calibration was observed with a mean value of 29 nm for gasoline, while Uy et al. [25] and La Rocca et al. [26] observed different mean values of dp_0, being 23 nm and 36 nm, respectively. Barone et al. [27] investigated the influence of the fuel injection timing on PM morphology using a blend of E20. The average primary particle diameter was found to be around 25 nm and ranged between 8 and 52 nm when the injection timing was advanced (i.e. 325 CAD bTDC from 303 CAD bTDC). The primary particle diameter was reduced to around 10-15 nm

when the fuel injection timing was retarded, but the range was widened when compared to advanced fuel injection timing (i.e. 7-60 nm). Similar results were observed by Lee et al. [28] in combustion studied with E20 with fuel injection timings ranging between 220 and 310 CAD bTDC.

The characterization of PM formed in GDI engines is still a subject under investigation in the automotive sector, especially when integrated within the hybrid vehicles where frequent stop starts are required. Understanding the particle characteristics is a key step for the development of efficient GPFs and accurate computational models in predicting their froation mechanism. The introduction of alternative fuel blends in the market (i.e. gasoline/bio-alcohols) can modify the physico-chemical properties of gasoline and consequently affect the PM morphological characteristics. The work for first time provides a detailed and comprehensive analysis on the impact of the combustion of the bio-alcohols on particle characteristics in GDI engines.

Materials and Methods

Experimental Setup and Procedure

A 2L air-guided, four-cylinder turbocharged GDI engine, which is a typical engine for mid-size/large family vehicles, has been used for this study. The engine specifications are listed in Table 1.

Table 1: GDI engine specifications

Engine Specifications	
Compression Ratio	10:1
Bore×Stroke	87.5× 83.1 mm
Turbocharger	Borg Warner k03
Rated Power	149 kW at 6000 rpm
Rated Torque	300 Nm at 1750-4500 rpm
Engine Management	Bosch ME 17

The fuels selected for the study were standard EN 228 gasoline and a blend composed of 75% (v/v) gasoline-25% (v/v) and ethanol (E25), both provided by Shell. Additionally, a blend composed of 67% (v/v) gasoline and 33% (v/v) butanol (B33) was prepared at the University of Birmingham. Both fuel blends B33 and E25 have the same oxygen content, hence the impact from the variability of the O_2 concentration can be eliminated and the influence of the fuels chemistry and physical properties on particulate formation can be obtained. The gasoline, ethanol and butanol fuel properties are shown in Table 2.

Table 2: Fuel Properties [21]

Property	**EN228**	**n-Butanol**	**Ethanol**
Chemical formula	$C_{5.88}H_{11.06}O_{0.1}$ [a]	$C_4H_{10}O$	C_2H_6O
Density (kg/m^3)	743.9 [a]	811	789
Research octane number (RON)	96.8 [a]	98	110
Motor octane number (MON)	85.2 [a]	85	90
Latent heat of vaporization (kJ/kg)	350	722	904
Lower Heat Value LHV (MJ/kg)	42.2 [a]	33.1	26.85
Laminar flame speed (cm/s)	51	58.5	63.6
Viscosity (mm^2/s) at 20℃	0.4-0.8	2.63	1.10

Adiabatic flame temperature (K)	2370	2340	2195

[a] *Provided by Shell*

For the PM morphology studies (i.e. primary particle diameter distribution, radius of gyration, number of primary particles and fractal dimension), 3.05 mm TAAB Formvar coated grids were used to collect the particles from the engine exhaust. The grids were directly exposed for short period of time to undiluted engine exhaust upstream the three-way catalyst. The paticles are collected on the grip through inertial deposition, a sampling method that provides high efficiency in collection of particles for TEM analysis [29]. A JEOL 1200 EX TEM LAB6 80Kev operating voltage was used to obtain the micrographs of particle agglomerates. Previous studies [25] show that the electron beam can modify PM or evaporate HCs; for this reason low voltage operation microscopy was utilised.

Particle size distribution (PSD) measurements were carried out using a TSI scanning mobility particle size (SMPS) composed by a 3080 electrostatic classifiers, a 3081 Differential Mobility Analyser (DMA) and a 3775 Condensation Particle Counter (CPC). The sample flow and the sheath flow were set to 1 and 10 lpm respectively. Consequently, the distribution ranged from 7.5 to 294 nm. The sampling point was located pre-TWC. To prevent HCs and water condensation, the line temperature was also maintained at 190 °C during the test. The samples were then diluted with air at a dilution ratio (DR) of 10, using an ejector diluter system, fitted with a high efficiency particle arrestance filter to precondition the air.

The fuels selected were tested at a steady-state condition of 60 Nm/2100 rpm (4.7 bar of IMEP) which is representative of urban driving conditions in the Worldwide Harmonized Light Vehicles Test Cycle (WLTC). Prior to the test, the engine was warmed up to 95±0.5 °C coolant and 95±2 °C oil temperature. The intake air stream temperature was maintained at 40±1 °C throughout the experiment to reduce the test-to-test variability. For the rest of engine parameters (i.e. injection timing or injection pressure), the standard Engine Control Unit (ECU) calibration settings were used in the test.

Morphological Analysis of Particle Emissions

The morphological analysis depends on the primary particle diameter (dp_0) since the radius of gyration (R_g), number of particles (n) and fractal dimension (D_f) are estimated from them. Measurements of primary particle size were performed only taking into account the most identifiable primary particles as in some cases the recognition of the primary particle boundaries could be subjective leading to misleading results [30]. In addition, the sample has to be sufficiently large to ensure its normality distribution as Gaddam et al. [31] discussed. On average approximately 1000 primary particles were measured from 30 different agglomerates per fuel blend. One-sample non-parametric Kolmogorov Smirnov test using a 5% significance on IBM statistical package for social sciences software (SPSS) was performed to check the normality of primary particle diameter distributions.

The number of primary particles (n) forming the agglomerates and radius of gyration (R_g) can be calculated based on literature expressions as follows:

Table 3: Calculation of particle number and radius of gyration

Number of Primary Particles	Radius of Gyration
$n = \left(\frac{A}{A_p}\right)^{\alpha}$ [32]	$R_g = \sqrt{\frac{1}{m}\sum r_i^2}$ [32]
n= Number of primary particles. A= The projected area from micrograph. A_p= Area of primary particle considered as circle. α= exponential factor for particle overlap 1.09 [28]	m= Number of pixel per agglomerate r= Distance between each pixel and the centroid of the agglomerate

Fractal dimension methods

Fractal dimension (D_f) of particles has been estimated using TEM micrographs. However, the overlapping of particles shown in the TEM micrographs can lead to inaccurate results. To avoid this, different methods have been developed [33-36]. In this work, three different methods have been evaluated to corroborate consistent tendencies.

The most used method to estimate D_f is known as fractal-equation or power law relationship, being defined by equation (1).

$$n = k_f \left(\frac{R_g}{dp_0}\right)^{D_f} \quad (1)$$

Where
n = Number of particles
k_f = Pre-factor term
R_g = Radius of gyration
dp_0 = Average of primary particle diameter

The power law relationship is only valid for agglomerates with self-similarities [37]. In this case, the fractal dimension can be estimated by evaluating the gradient of a linear regression line that fits with data for ln (n) versus ln (R_g/dp_0) according to expression (2):

$$\ln(n) = \ln(k_f) + D_f \ln\left(\frac{R_g}{dp_0}\right) \quad (2)$$

Minimum Bounding Rectangle Method (MBR) has also been used to determine the fractal dimension. This method is based on bounding the agglomerate with a minimal surface, thereby, each minimum bounding rectangle is defined by its length L, and width W. In this way, the radius of gyration can also be estimated from a characteristic length derived from the surface area of the minimum bounding rectangle, being $\sqrt{LW}$. Therefore, D_f can be estimated through equation (3):

$$\ln(n) = \ln(k_f) + D_f \ln\left(\frac{\sqrt{LW}}{dp_0}\right) \quad (3)$$

Root Form Factor (RFF) is a non-dimensional parameter that represents the ratio area-perimeter of the agglomerate. RFF has been reported to be comparable to fractal dimension, and is defined by equation (4):

$$RFF = \sqrt{\frac{4\pi A_p}{Perimeter^2}} \quad (4)$$

Prior to the morphological analysis, the TEM micrographs were pre-treated using Matlab. This pre-treatment consists of background removal to binarise the TEM micrographs. An in-house Matlab code was implemented to estimate radius of gyration, the number of primary particles, fractal dimension and RFF from the TEM micrographs. This algorithm was developed following the methodologies described in literature for morphological characteristics analysis of PM [30, 38].

Results and Discussion

Primary particle size distributions

Particles from the combustion of gasoline have an aciniform-shape and are composed by several near-spherical primary particles. Representative examples of TEM micrographs are shown in Figure 1. The combustion of B33, provides agglomerated particles with wide variability in nature, a trend which is in agreement with the results previously reported in literature for the gasoline combustion [4]. It was observed that the particles nature can be: i) HCs droplets that can mainly be composed of elemental carbon and some traces of oil metals [39], ii) small solid agglomerates composed by a low number of primary particles, iii) 'wet' agglomerates particles, which are a combination of solid particles and liquid unburned hydrocarbons and iv) fractal-like particles, similar to the particles emitted in diesel engines. The TEM micrographs of the particles from the combustion of E25 were mainly found to be fractal-like particles and some small HCs droplets. The presence of large agglomerates (Figure 2) in the engine exhaust gas, are only seen in the combustion of gasoline and B33.

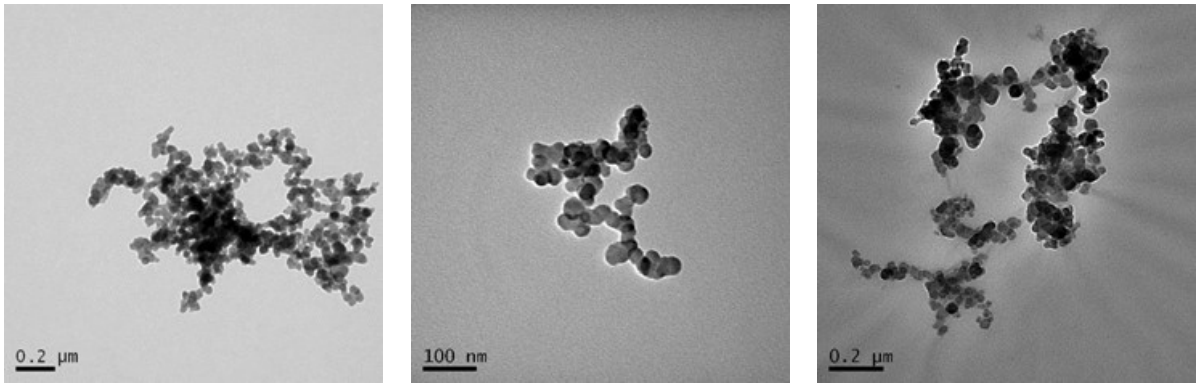

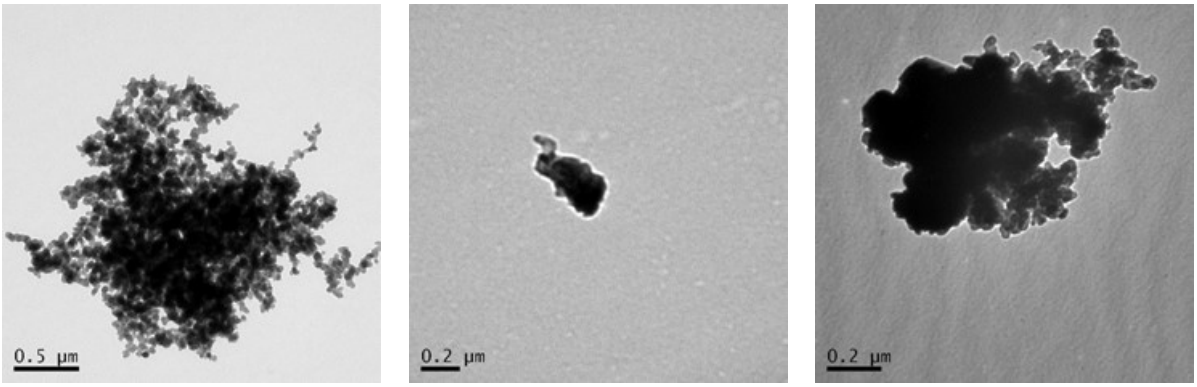

a) b) c)

Figure 1. TEM micrographs of particles for: a) Gasoline, b) E25 and c) B33.

a) b)

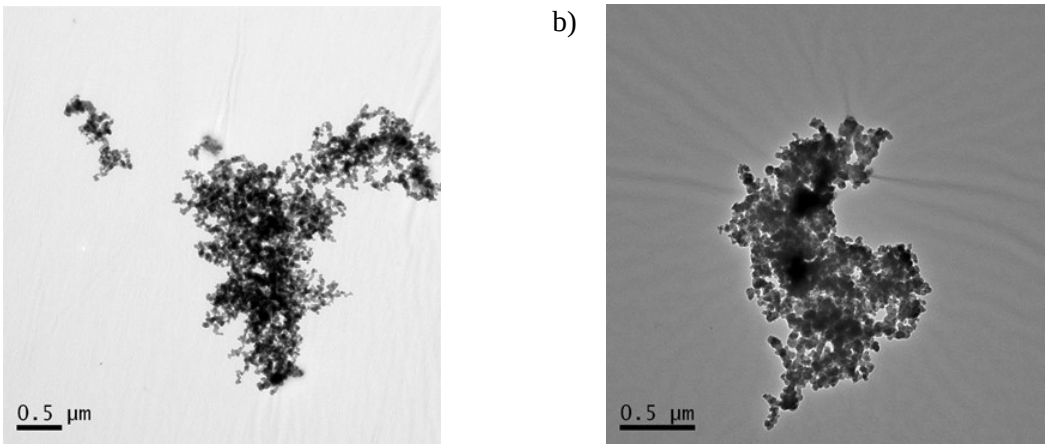

Figure 2. Large agglomerates: a) Gasoline and b) B33.

The primary particle size (dp_0) distributions obtained from the combustion of the three fuels (Figure 3) present a larger standard deviation than in the case of particles produced by compression ignition engines [27], demonstrating the variability of particles from GDI engines. The one-sample non-parametric Kolmogorov Smirnov test verified that the primary particle diameter samples for the three fuels satisfied the normality test (Table 4).

Table 4. Statistical normality test

Fuel	Test	Statics	Decision at level (5%)
Gasoline	One-sample Kolmogorov Smirnov	0.0332	Normal distribution
E25		0.0497	Normal distribution
B33		0.02974	Normal distribution

The results from the combustion of B33 and gasoline, suggest that there is a compensation between beneficial and negative physico-chemical properties affecting primary particles size, which results in comparable dp_0 distributions. However, a reduction in primary particle diameter for B33 was expected due to the oxygen present in the butanol molecule [40]. These results suggest that other thermo-

physical fuel properties, mainly those affecting fuel spray pattern and in-cylinder temperature (i.e. fuel injection strategies, fuel viscosity and fuel latent heat of vaporisation), have a significant role on soot and primary particles size production.

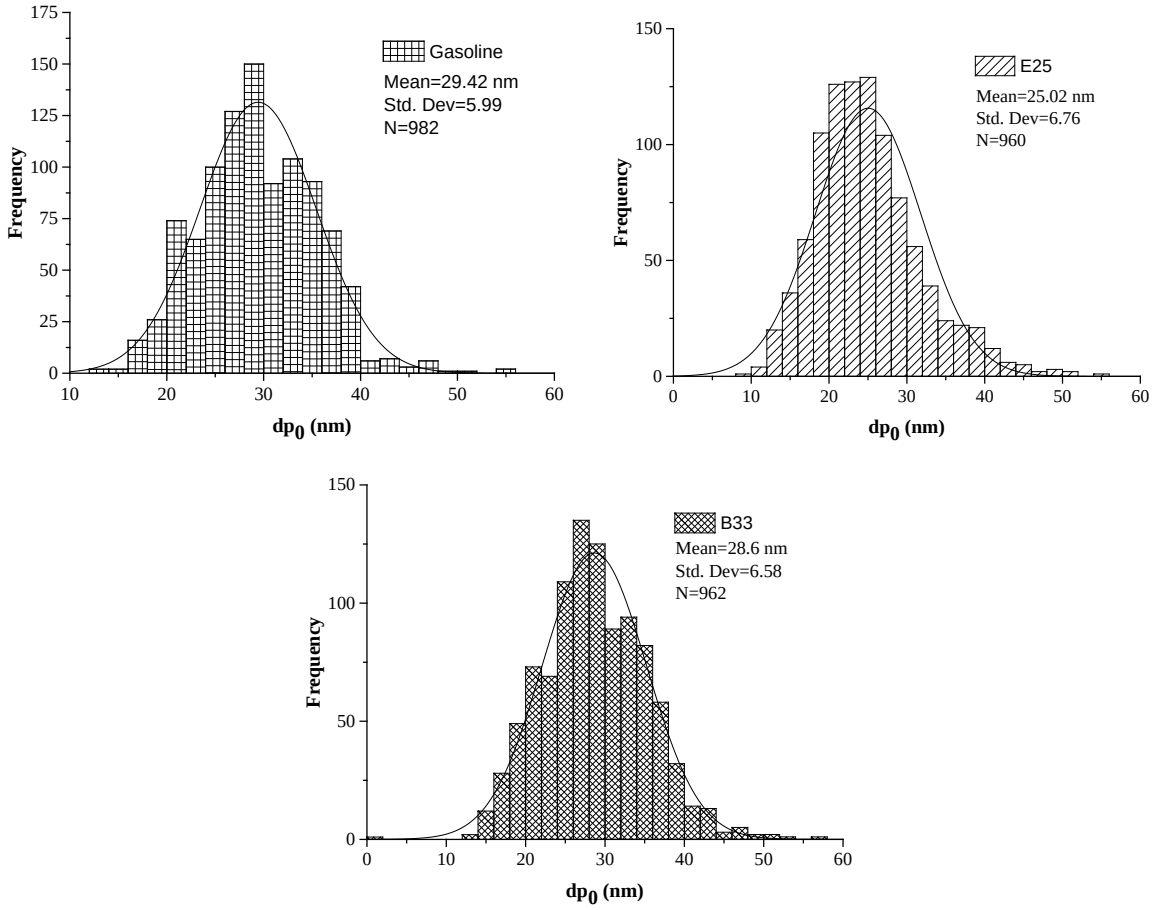

Figure 3. Primary particle size distributions for: a) Gasoline, b) E25 and c) B33.

Therefore, a comprehensive analysis considering the sources of particle formation, fuel spray patterns, fuels chemical and physical properties and the threshold temperature for soot formation, is required in udersanding the effect of alcohols on particles formation during combustion. For instance, it has been reported by Hageman et al. [41] that temperatures above 1800 K prevent soot formation, as the temperature is sufficiently high to oxidise soot precursors (i.e. acetylene) that slow down benzene formation, and thus the development of larger particles. The maximum rate of soot formation was found to lie between the temperature range of 1500 K and 1600 K, and air fuel ratio of 1.5-1.8.

The higher viscosity of butanol (≈ 4 times higher than gasoline) can reduce the quality of the fuel spray [42], while the higher amount of fuel required to maintain the same engine brake power (Figure 4 (a)), on account of its lower energy density (common for bio-alcohols fuels). Therefore, the spray penetration length may increase, resulting in fuel droplets that are more difficult to break-up [43]. This can lead to a considerable number of isolated locally fuel rich regions and piston wetting spots. This liquid-phase portion of fuel spray impinges on the piston wall prior to the formation of the flame,

so fuel films can be accumulated on the wall. Then, this film is poorly burned, in rich, late-burning and soot-forming flames. The higher heat of vaporisation of butanol (≈ 2 times higher than gasoline) cools the combustion chamber resulting in lower temperatures which also worsen fuel vaporisation [18], particularly on the piston and/or cylinder where the fuel rich surfaces can promote the presence of soot precursors. This particle formation process in the case of butanol is expected to promote primary particles growth. This is as a consequence of the combustion conditions, favour particle nucleation (high temperatures) and surface growth (isolate rich areas) [5], in which hydrocarbon in gas phase and hydrocarbon fragment are accreted to the nuclei, leading to a planar growth of PAH. Additionally, coagulation mechanism can take place as the likely elevated combustion temperatures for B33 combustion can lead to high kinetic energy of the primary particles increasing there mobility, and therefore, the probability of collisions between primary particles. This mechanism can increase the primary particle diameter but promoting a significant reduction of the number of particles. Brake specific fuel consumption (Figure 4 (a)) of bio-alcohols blends is higher compare to gasoline fuel combustion. However, when brake thermal efficiency is calculated, which take into account the lower calorific value of the alcohol fuels, all three fuels present comparable engine brake thermal efficiency (Figure 4 (b)). It has been also reported in the literature that the faster flame velocity of bio-alcohols [44], which leads to the flame develops upon a narrower number of crank degree angles, and reflected in slightly advanced combustion observed from the mass fraction burned (MFB) patterns in Figure 5 (a). This can improve combustion quality (Figure 5 (b)), and promote higher in-cylinder pressure (Figure 6 (a)), which increases in-cylinder temperatures.

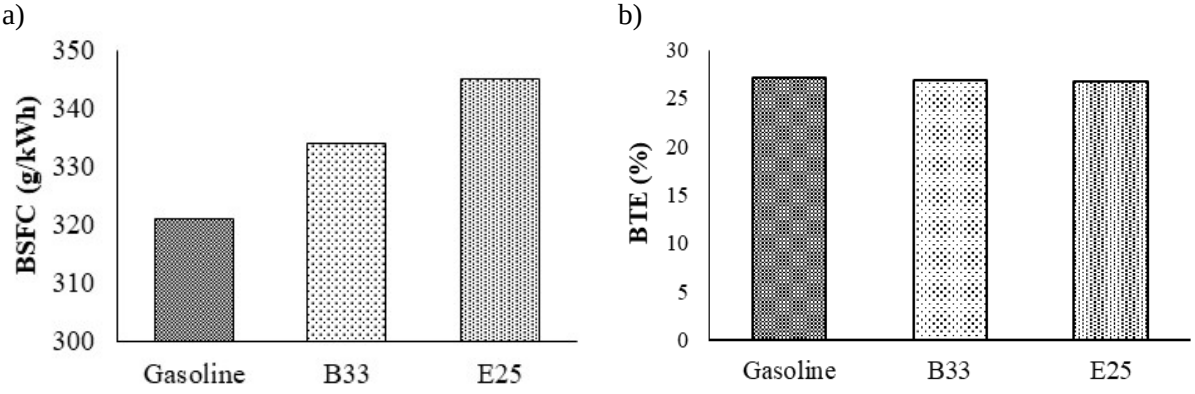

Figure 4. a) Brake Specific Fuel Consumption (BSFC), and b) Brake Thermal Efficiency (BTE).

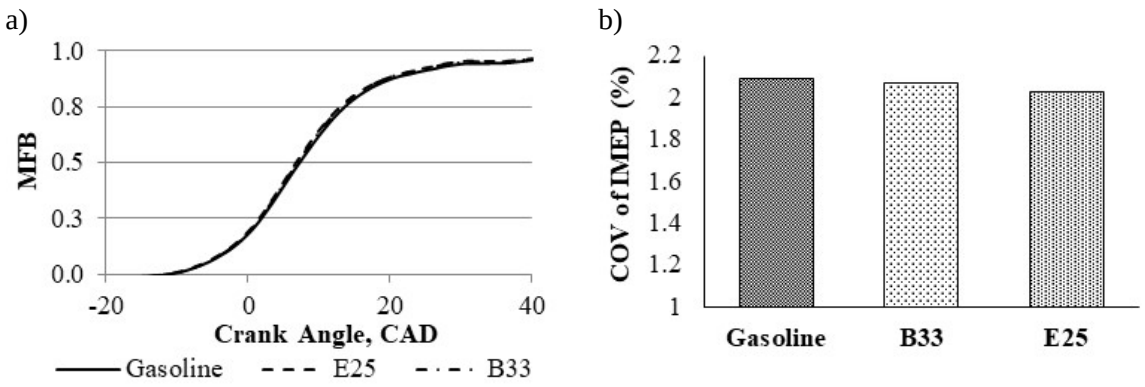

Figure 5. a) Mass Fraction Burned (MFB) and b) COV of IMEP (%) for gasoline, E25 and B33.

The higher exhaust temperatures measured in the case of B33 with respect to gasoline combustion (Figure 6 (b)) could be an indication of higher in-cylinder temperatures [45]. Although, higher temperatures can lead to higher level of nucleation, elevated temperature promotes greater oxidation rates during the combustion and exhaust strokes, This can completely oxidise the majority of the soot precursors located in the rich pockets of the different hydrocarbons, and thus competing against the primary particle growth [45].

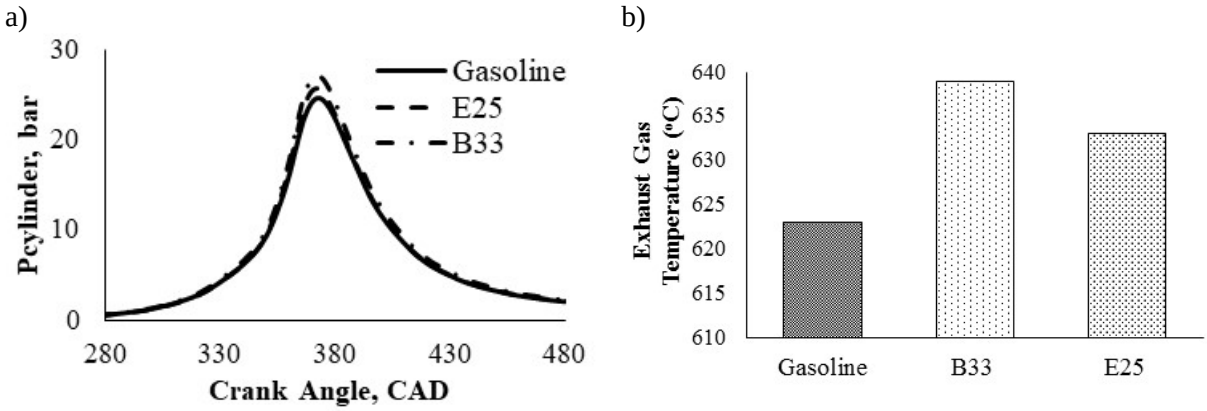

Figure 6. a) in-cylinder pressure and b) Exhaust gas temperature for Gasoline, B33 and E25.

Therefore, the higher oxygen content and the reduction of aromatic components in B33 combined with the likely higher in-cylinder temperatures seems to counteract the higher viscosity and latent heat of vaporisation of butanol and consequently, maintain the primary particle size in a similar or slightly smaller range than those emitted by gasoline fuel. For the E25 combustion, the primary particulate distribution is shifted to smaller diameters with respect to B33 and gasoline (Figure 3). Ethanol in the fuel blend provides advantageous thermo-physical properties when compared to butanol combustion that lead in the reduced formation of the primary particles. For instance, and in contrast with butanol, the viscosity of ethanol is lower compared to butanol, which has been reported to lead to lower spray momentum and piston wetting [46]. This effect can favour better quality of air-fuel mixture and quicker initial evaporation with respect to B33 [43]. Consequently, the improved spray pattern can further enhance the air-fuel mixture homogeneity, can reduce incomplete combustion, and thus may

decrease the accretion of hydrocarbons to the nuclei particle, reducing its growth [6, 19]. E25 fuel was also selected to eliminate the impact of non-ideal behaviour seen from the combustion of the ethanol/gasoline blends with up to 20% ethanol by volume [47]. In this specific ethanol/gasoline ratio, the vapour pressure of the mixture does not behave linearly with the increase in ethanol content and Raoult's law is not applicable. The elimination of non-ideal behaviour favours the mixture of ethanol with gasoline hydrocarbons and therefore, this aspect can potentially improve the evaporation of E25 in the combustion chamber with respect to B33, being helpful to reduce fuel rich regions and fuel impingement. Accordingly, the improvement in fuel spray patterns and subsequent reduction of soot sources (i.e. PAH content) will enable to the oxygen content in the ethanol molecule to inhibit primary particle formation rate and enhance oxidation compared to B33 and gasoline (Figure 3). In addition, E25 has higher overall H/C ratio, containing light and short chain hydrocarbons, which are readily oxidised and are less associated with particulate formation.

The average primary particle size (dp_0) and standard deviation from the combustion of the three fuels are presented in Figure 7. The dp_0 is also related with soot oxidation reactivity, as it is dependent on the aggregate surface area to volume ratio. Therefore, small primary particle diameters will lead to low aggregate surface area favouring soot oxidation [48]. The average primary particle size dp_0 is 29.42 nm, 28.60 nm and 25 nm from the combustion of gasoline, B33 and E25, respectively.

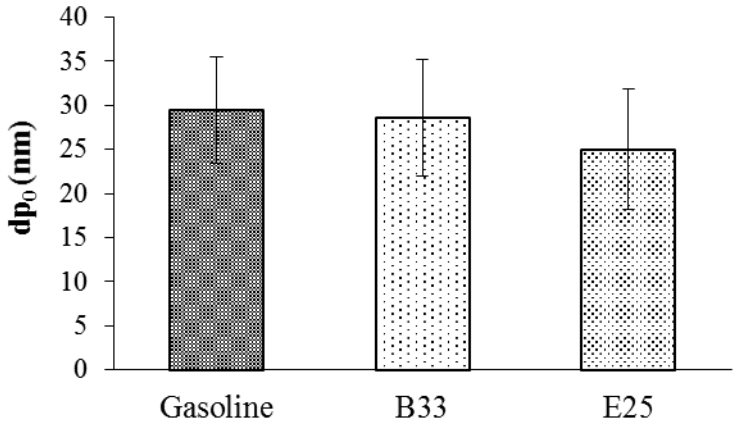

Figure 7. Average primary particle diameter (dp_0).

Combustion B33 fuel belnd slightly reduces the average dp_0 but the standard deviation error bar is almost overlap, indicating that the diameter of the primary particles formed from the combustion of gasoline and B33 are similar. The combustion of E25 resulted in a reduction of approximately 3nm in the diameter of the primary particle, as the standard deviation error does not overlap with gasoline and B33. It is required to highlight that the main range of primary particle sizes at sub-micron morphology level in this study is between 23-35 nm, thereby, a reduction of 3 nm is significant for morphological features. Any differences attributed to measurement uncertainties were reduced at maximum due to exclusive consider the most recognizable primary particles in the agglomerates. Thus, it can be

concluded that the observed reduction in primary particles size emitted from the combustion of E25 is a consequence of the properties of this blend. Additionally, smaller primary particle sizes increases the surface area to volume ratio, which can improve soot oxidation reactivity , which is key factor to increase the efficiency of GPF regeneration process.

Aggregate PSD, radius of gyration and number of primary particles

In this section, the analysis of the average number of primary particles per agglomerate, the radius of gyration and the particle size distributions from the combustion of the three fuels is presented. The particle size distributions (Figure 8) show that the combustion of gasoline leads to production of larger particles compared to the other two fuel blends. The most significant reduction of 80% in the PM peak concentration was achieved in the combustion of B33, when compared to gasoline. The maximum particle concentration was 30% lower from the combustion of E25 when compared to gasoline, but E25 emitted the highest concentration of smaller particles in the range between 7 nm and 40 nm. E25 emitted the lowest concentration of PM within the range of 100-300 nm; this result can explain the lack of large agglomerates observed in the TEM micrographs (Figure 2). Additionally, E25 gives the lowest geometric number mean diameter (GNMD) of the agglomerate (35 nm) follow by B33 (50 nm) and gasoline (67 nm).

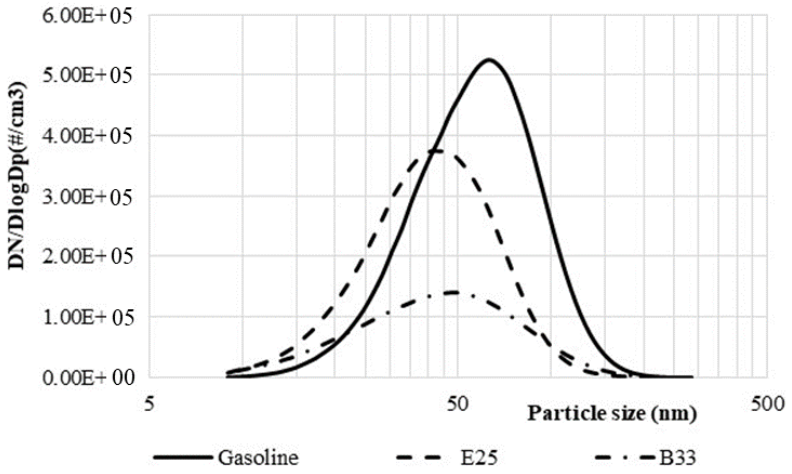

Figure 8. Particle size distribution for Gasoline, E25 and B33.

The size of the agglomerates and the number of primary particles depends on the competition between nucleation and oxidation mechanisms during the fuel combustion process. The nucleation mechanism for soot formation is highly related to the temperature as has been discussed in the previous section.

The impact of fuel used on the particle radius of gyration (*Rg*), as obtained from the TEM micrographs, and the number of primary particles per agglomerate (Figure 9) follows the order of: gasoline>B33>E25. The trend in radius of gyration agrees with GNMD results obtained from the particle size distributions (Figure 8), and coincides with the trend seen in the size of primary particles (Figure 7). The radius of gyration measured using TEM micrographs (Figure 9 (a)) is larger than that

of the equivalent diameters measured by the mobility scanning sizer [45, 49], but the trends are again consistent. It is observed from the results that the presence of large agglomerates emitted by gasoline combustion increases both radius of gyration and primary particles per agglomerate. In addition, the variability (large standard deviation) is higher compared to B33 and E25. This observation is consistent with the lower gasoline combustion stability, which results in the production of wider size particles. According to literature [4], the vaporisation of light components of the gasoline can leave heavy fraction of gasoline more prone to soot precursor formation (i.e. higher content of aromatics) during the expansion stroke. Those particles are produced in fuel rich regions, with high concentration and increased probabilities of collions between them. This trend leads in particle emissions with increased radius of gyration. Conversely, even though the B33 gives larger agglomerates composed of a higher number of particles in comparison to E25, the concentration of particles was found to be the lowest (Figure 8). Therefore, it is proposed based on the results, that the higher in-cylinder pressure and exhaust temperatures observed during B33 combustion process (Figure 6 (a) and (b)), can promote further soot oxidation and post-oxidation, leading the significant reduction of particle concentration [22]. Additionally, BSFC was also the highest for E25 (Figure 4 (a)), resulting in greater amount of fuel in the combustion chamber that will proportionally increase the concentration of small particles (i.e. 7 nm-43 nm) relatively to B33 and gasoline.

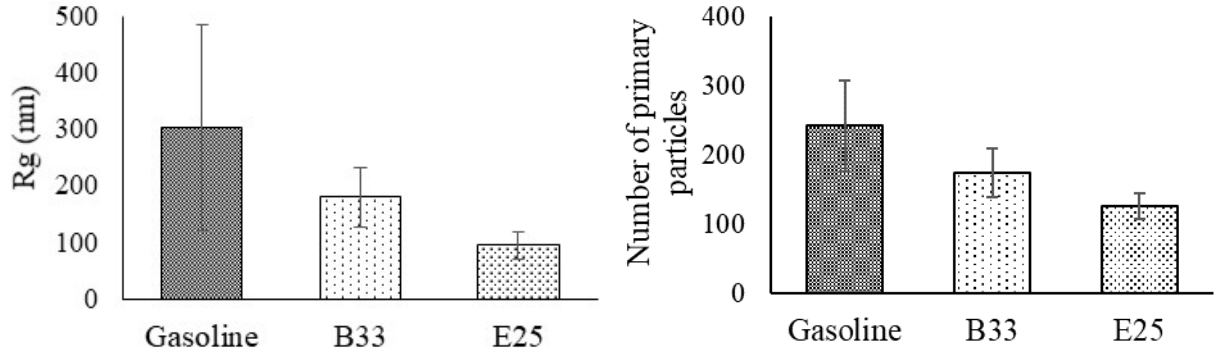

Figure 9. Morphological Parameters: a) Radius of Gyration (nm) and b) Number of primary particles per agglomerate.

Although, fuel rich pockets and piston wetting is difficult to avoid in GDI technology, due to the nature of the spray, the properties of bio-alcohols such as oxygen content, lower aromatics and high laminar flame velocity have a positive effect in reducing the particulate concentration. In addition, the physico-chemical properties also provide a significant impact on particles formation, which also strongly affects the nature of the PM formed in GDI engines.

Fractal Dimension D_f

The three different methods that are commonly used in literature for estimated of fractal dimension are used and compared in this investigation for the fuels. Calculating the fractal dimension with power law relationship tends to underestimate the value while using minimum bounding rectangle provides more accurate and sensitive to change of fuels and engine conditions. The root factor form presents a wide standard deviation for gasoline and B33, which indicates more variety of agglomerates emitted for those fuels, while for E25 is significantly reduced, supporting less variability in the nature of the agglomerates. Gasoline combustion produces the most compact agglomerates with a fractal dimension of 1.7-1.75 whilst the B33 seems to provide similar or slightly lower D_f when compared to gasoline, a result that is not totally conclusive (Figure 10). Although E25 and B33 have the same concentration of oxygen, the particulate fractal dimension D_f, from the combustion of E25 is notably lower, meaning E25 produces more chain-like agglomerates compared to gasoline and B33.

In addition, D_f not only expresses the result of the collisions, but also the type of collisions the particles can likely experience [50]. It has been reported that the collision of particles depends on the interplay of particle section and particle velocity, and on whether the collisions involves spherules and agglomerates, or just agglomerates [50]. In the case of E25, the growth of primary particles was observed to be lower than gasoline and B33 as well as the radius of gyration, but with a higher number concentration. Therefore, the mean free path for E25 will be smaller than the agglomerate, which promotes a 'diffusion-limit' growth, where the spherules are attached to outer regions, resulting in chained morphologies [51]. Conversely, for B33 and gasoline, predominant growth could be 'ballistic' where the spherules penetrate to the interior regions of the agglomerate, leading to more cluster morphologies. These type of collisions are found when the mean free path is larger than the agglomerates [51]. The higher fractal dimensions observed for particles emitted with the combustion of gasoline and B33 increases the effective density of particles and thus, the surface reactive area in contact with lungs [23].

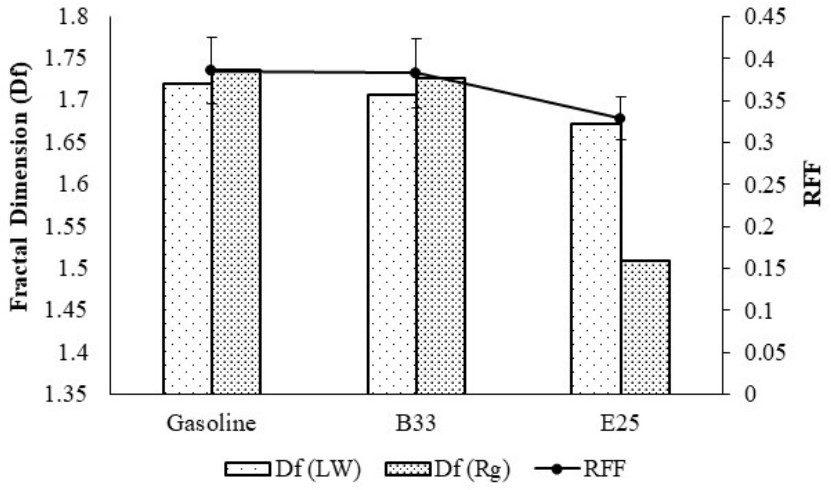

Figure 10: Fractal Dimension calculated with different methods.

Conclusions

A novel and comprehensive morphological analysis of particulate matter emitted by a gasoline direct injection engine from the combustion of gasoline and gasoline blended with ethanol and butanol B33 has been carried out in this work. Statistical analysis and well-established methods for calculating the fractal dimension of particles have been used to ensure the normality and significance/reliability of the results and trends.

Due to the physico-chemical properties, such as oxygen content, laminar speed velocity or lighter hydrocarbon chains, the combustion of bio-alcohol fuels have a tendency in reducing primary particle diameters, where ethanol-gasoline blend emitted the smallest in comparison to butanol-gasoline fuel and commercial gasoline. The bio-alcohol benefits were also observed in the significant reduction of particle concentration, being up to 80% with B33 case in comparison to gasoline as well as lower agglomerate size, which is reflected in slightly smaller radius of gyration. The fractal dimension shows a reduction with the combustion of bio-alcohols, being more significant for E25 than B33, which indicates more like-chain agglomerates. Despite of the reduction of particle number concentration by butanol-gasoline blend, these agglomerates were larger and more compact with respect to E25. The lower concentration of particles and radius of gyration may have a positive influence in filter technology as it will reduce the accumulation of particles in GPF. This may result in lower pressure drop and frequency of regeneration, further enhancing fuel economy in comparison to gasoline particle emissions. While the smaller primary particle diameters can result in higher reactivity due to greater particle surface/volume ratio (reducing the energy for gasoline particle filter regeneration strategies), particles with low fractal dimension has high potential to be readily trapped in the filters.

Acknowledgments

The work has been funded by the European Union's Horizon 2020 research and innovation programme as part of the PARTIAL PGMs grant No 686086. C.H. would like to thank University of Birmingham for his scholarship. Innovate UK (Technology Strategy Board) is also acknowledged for supporting this work with the project "CO2 Reduction through Emissions Optimisation" (CREO: ref. 400176/149).

References

1. Fennell, D., et al., Thermochemical recovery technology for improved modern engine fuel economy - part 1: analysis of a prototype exhaust gas fuel reformer. *RSC Advances*, 2015. **5**(44): p. 35252-35261.
2. Velji, A., et al. Investigations of the Formation and Oxidation of Soot Inside a Direct Injection Spark Ignition Engine Using Advanced Laser-Techniques, SAE International, 2010-01-0352, 2010.
3. Zhang, M., et al., Combustion, performance and particulate matter emissions analysis of operating parameters on a GDI engine by traditional experimental investigation and Taguchi method. *Energy Conversion and Management*, 2018. **164**: p. 344-352.

4. Bogarra, M., et al., Impact of exhaust gas fuel reforming and exhaust gas recirculation on particulate matter morphology in Gasoline Direct Injection Engine. *J. Aerosol Sci.*, 2017. **103**: p. 1-14.
5. Pfau, S.A., et al., Comparative nanostructure analysis of gasoline turbocharged direct injection and diesel soot-in-oil with carbon black. *Carbon*, 2018. **139**: p. 342-352.
6. Eastwood, P., *Formation I: Composition*, in *Particulate Emissions from Vehicles*. 2008, John Wiley & Sons, Ltd.
7. Mamakos, A., et al., Cost effectiveness of particulate filter installation on Direct Injection Gasoline vehicles. *Atmos. Environ.*, 2013. **77**: p. 16-23.
8. Hergueta, C., et al., Butanol-gasoline blend and exhaust gas recirculation, impact on GDI engine emissions. *Fuel*, 2017. **208**: p. 662-672.
9. Chan, T.W., et al., Evaluation of a Gasoline Particulate Filter to Reduce Particle Emissions from a Gasoline Direct Injection Vehicle. *SAE Int. J. Fuels Lubr.*, 2012. **5**(3): p. 1277-1290.
10. Richter, J.M., et al., Application of Catalyzed Gasoline Particulate Filters to GDI Vehicles. *SAE Int. J. Engines* 2012. **5**(3): p. 1361-1370.
11. Bogarra, M., et al., Study of particulate matter and gaseous emissions in gasoline direct injection engine using on-board exhaust gas fuel reforming. *Appl. Energ*, 2016. **180**: p. 245-255.
12. Fennell, D., J. Herreros, and A. Tsolakis, Improving gasoline direct injection (GDI) engine efficiency and emissions with hydrogen from exhaust gas fuel reforming. *Int. J. Hydrogen Energ*, 2014. **39**(10): p. 5153-5162.
13. Heyne, S. and S. Harvey, Assessment of the energy and economic performance of second generation biofuel production processes using energy market scenarios. *Appl.Energ*, 2013. **101**: p. 203-212.
14. Leung, P., et al., Raising the fuel heating value and recovering exhaust heat by on-board oxidative reforming of bioethanol. *Energ. Environ. Sci.*, 2010. **3**(6): p. 780-788.
15. Yu, X., et al., Effect of gasoline/n-butanol blends on gaseous and particle emissions from an SI direct injection engine. *Fuel*, 2018. **229**: p. 1-10.
16. Barrientos, E.J., et al., Particulate matter indices using fuel smoke point for vehicle emissions with gasoline, ethanol blends, and butanol blends. *Combust.Flame*, 2016. **167**: p. 308-319.
17. Niass, T., et al., Butanol Blending - a Promising Approach to Enhance the Thermodynamic Potential of Gasoline - Part 1. *Int. J. Fuels Lubr.*, 2011. **5**(1): p. 265-273.
18. Broustail, G., et al., Comparison of regulated and non-regulated pollutants with iso-octane/butanol and iso-octane/ethanol blends in a port-fuel injection Spark-Ignition engine. *Fuel*, 2012. **94**: p. 251-261.
19. Luo, Y., et al., Size distribution, chemical composition and oxidation reactivity of particulate matter from gasoline direct injection (GDI) engine fueled with ethanol-gasoline fuel. *Appl. Therm. Eng.*, 2015. **89**: p. 647-655.
20. He, X., et al. The Impacts of Mid-level Biofuel Content in Gasoline on SIDI Engine-out and Tailpipe Particulate Matter Emissions, SAE International, 2010-01-2125, 2010.
21. Zhang, Z., et al., Combustion and particle number emissions of a direct injection spark ignition engine operating on ethanol/gasoline and n-butanol/gasoline blends with exhaust gas recirculation. *Fuel*, 2014. **130**: p. 177-188.
22. Lattimore, T., et al., Investigation of compression ratio and fuel effect on combustion and PM emissions in a DISI engine. *Fuel*, 2016. **169**: p. 68-78.
23. Broday, D.M. and R. Rosenzweig, Deposition of fractal-like soot aggregates in the human respiratory tract. *J. Aerosol Sci.*, 2011. **42**(6): p. 372-386.
24. Barone, T.L., et al., Inertial deposition of nanoparticle chain aggregates: Theory and comparison with impactor data for ultrafine atmospheric aerosols. *J. Nanopart. Res.*, 2006. **8**(5): p. 669-680.
25. Uy, D., et al., Characterization of gasoline soot and comparison to diesel soot: Morphology, chemistry, and wear. *Tribol. Int.*, 2014. **80**: p. 198-209.
26. La Rocca, A., et al., Characterisation of soot in oil from a gasoline direct injection engine using Transmission Electron Microscopy. *Tribol. Int.*, 2015. **86**: p. 77-84.
27. Barone, T.L., et al., An analysis of direct-injection spark-ignition (DISI) soot morphology. *Atmos. Environ.*, 2012. **49**: p. 268-274.
28. Lee, K.O., et al. Detailed Morphological Properties of Nanoparticles from Gasoline Direct Injection Engine Combustion of Ethanol Blends, SAE International, 2013-24-0185, 2013.
29. Bogarra, M., et al., Influence of on-board produced hydrogen and three way catalyst on soot nanostructure in Gasoline Direct Injection engines. *Carbon*, 2017. **120**: p. 326-336.
30. Kondo, K., et al. Uncertainty in Sampling and TEM Analysis of Soot Particles in Diesel Spray Flame, SAE International, 2013-01-0908, 2013.

31. Gaddam, C.K. and R.L. Vander Wal, Physical and chemical characterization of SIDI engine particulates. *Comb. Flame*, 2013. **160**(11): p. 2517-2528.
32. Megaridis, C.M. and R.A. Dobbins, Morphological Description of Flame-Generated Materials. *Comb. Sci. Technol.*, 1990. **71**(1-3): p. 95-109.
33. Lapuerta, M., R. Ballesteros, and F.J. Martos, A method to determine the fractal dimension of diesel soot agglomerates. *J. Colloid Interface Sci.*, 2006. **303**(1): p. 149-158.
34. Zurita-Gotor, M. and D.E. Rosner, Effective Diameters for Collisions of Fractal-like Aggregates: Recommendations for Improved Aerosol Coagulation Frequency Predictions. *J. Colloid Interface Sci.*, 2002. **255**(1): p. 10-26.
35. Wozniak, M., et al., Comparison of methods to derive morphological parameters of multi-fractal samples of particle aggregates from TEM images. *J. Aerosol Sci.*, 2012. **47**: p. 12-26.
36. Chakrabarty, R.K., et al., Structural and Fractal Properties of Particles Emitted from Spark Ignition Engines. *Environ. Sci. Technol.*, 2006. **40**(21): p. 6647-6654.
37. Theiler, J., Estimating fractal dimension. *J. Opt. Soc. Am.*, 1990. **7**(6): p. 1055-1073.
38. Lottin, D., et al., On methods determining the fractal dimension of combustion aerosols and particleclusters. *J. Aerosol Sci.*, 2013. **58**: p. 41-49.
39. Karjalainen, P., et al., Exhaust particles of modern gasoline vehicles: A laboratory and an on-road study. *Atmos. Environ.*, 2014. **97**: p. 262-270.
40. Fayad, M.A., et al., Manipulating modern diesel engine particulate emission characteristics through butanol fuel blending and fuel injection strategies for efficient diesel oxidation catalysts. *Appl. Energ.*, 2017. **190**: p. 490-500.
41. Hageman, M.D., S.S. Sakai, and D.A. Rothamer, Determination of soot onset and background particulate levels in a spark-ignition engine. *Proc. Combust. Inst.*, 2015. **35**(3): p. 2949-2956.
42. Irimescu, A., et al., Combustion process investigations in an optically accessible DISI engine fuelled with n-butanol during part load operation. *Renew.Energ*, 2015. **77**: p. 363-376.
43. Aleiferis, P.G. and Z.R. van Romunde, An analysis of spray development with iso-octane, n-pentane, gasoline, ethanol and n-butanol from a multi-hole injector under hot fuel conditions. *Fuel*, 2013. **105**: p. 143-168.
44. Duan, X., et al., Influence of single injection and two-stagnation injection strategy on thermodynamic process and performance of a turbocharged direct-injection spark-ignition engine fuelled with ethanol and gasoline blend. *Appl. Energ.*, 2018. **228**: p. 942-953.
45. Zhu, J., et al., Effects of engine operating conditions on morphology, microstructure, and fractal geometry of light-duty diesel engine particulates. *Proc. Combust. Inst.*, 2005. **30**(2): p. 2781-2789.
46. Storch, M., et al., The effect of ethanol blending on mixture formation, combustion and soot emission studied in an optical DISI engine. *Appl. Energ.*, 2015. **156**: p. 783-792.
47. Kar, K., et al., Measurement of Vapor Pressures and Enthalpies of Vaporization of Gasoline and Ethanol Blends and Their Effects on Mixture Preparation in an SI Engine. *SAE Int. J. Fuels Lubr.*, 2008. **1**(1): p. 132-144.
48. Pahalagedara, L., et al., Structure and Oxidation Activity Correlations for Carbon Blacks and Diesel Soot. *Energy & Fuels*, 2012. **26**(11): p. 6757-6764.
49. Abdul-Khalek, I.S., et al. Diesel Exhaust Particle Size: Measurement Issues and Trends, SAE International, 980525, 1998.
50. Harris, S.J. and M.M. Maricq, Signature size distributions for diesel and gasoline engine exhaust particulate matter. *J. Aerosol Sci.*, 2001. **32**(6): p. 749-764.
51. Lee, K.O., et al. Detailed Characterization of Morphology and Dimensions of Diesel Particulates via Thermophoretic Sampling, SAE International, 2001-01-3572, 2001.